Syntheses of monodispersed SnO_2 and CeO_2 nanoparticles through the self-capping role of 2-ethylhexanoate ligands†

Yong Joo Kim, Young Seok Kim, Seung Yong Chai, Dong Hyun Cha, Young Sik Choi and Wan In Lee*

Received (in Montpellier, France) 5th July 2006, Accepted 25th September 2006
First published as an Advance Article on the web 22nd December 2006
DOI: 10.1039/b609577a

Monodispersed 2.4 nm-sized SnO_2 and 2.6 nm-sized CeO_2 nanoparticles have been reproducibly formed through a non-hydrolytic solvothermal reaction with 2-ethylhexanoate complexes, without the addition of extra surfactants. During the synthesis, the dissociated 2-ethylhexanoates from the central metals work as a capping agent, and this induces size control of the nanoparticles and the suppression of interparticular aggregation. The as-prepared nanoparticles are soluble in a non-polar solvents, and by converting the capping group to a citrate, they also form transparent suspensions in an aqueous solution. The as-synthesized SnO_2 nanoparticles are of the pure cassiterite structure, while those of the CeO_2 are of the calcium fluoride structure. X-Ray photoelectron spectroscopy (XPS) analysis indicates that the oxidation state of the Sn and Ce are close to +4. The band gaps of SnO_2 and CeO_2 nanoparticles are 4.14 and 3.68 eV, respectively, which are relatively large values because of the quantum size effect.

Introduction

Recently, the reverse micelle process has been widely applied in the syntheses of nanoparticles for various metals[1–4] and semiconductors.[5–7] Carboxylic acids or amines with long hydrocarbon chains form a stable reverse micelle array in non-polar ethers, and the cavities inside these arrays can be used as nanoreactors for the formation of quantum-sized nanoparticles.[8,9] In particular, for the preparation of metal oxide nanoparticles, the carboxylic acids with long chain alkyl groups are expected to act as suitable surfactants, considering their strong binding affinity towards metal oxides.[10,11]

In this work we report a synthetic method for preparing SnO_2 and CeO_2 nanoparticles from 2-ethylhexanoate complexes without adding surfactant or stabilizer. When the metal carboxylates with long hydrocarbon chains, dissolved in a non-polar solvent, are heated at an elevated temperature, the carboxylate ligands will become dissociated from the central metal. Then, the released ligands can surround it like a surfactant, and the growth of nuclei to large particles or aggregations between the particles will be suppressed automatically. This synthetic route is a kind of the non-hydrolytic decomposition reaction initially suggested by M. Niederberger *et al.*[12,13] Previously, 2-ethylhexanoate complexes were used in the formation of CdS nanoparticles[14] and in the sonochemical synthesis of $BaFe_{12}O_{19}$,[15] but in these cases, the role of 2-ethylhexanoate in controlling particle size was not clear, since the synthesized nanoparticles were not the simple binary metal oxide. Recently, M. Epifani *et al.* reported the preparation of SnO_2 and ZnO nanoparticles from 2-ethylhexanoate complexes.[16] However, in their reactions, several alkylamines were added as capping agents, and they reported that the size of the prepared nanoparticles was dependent on the length of the alkyl chain of the amines.

In metal 2-ethylhexanoates, the ratios of metal-to-ligand are generally 1 : 2–1 : 6. In conventional reverse micelle processes, the typical molar ratio of the metal precursor to the surfactant is in the range 1 : 1–1 : 10.[17] This suggests that the molarity of the organic fragments dissociated from the metal precursor is comparable to that of the surfactants. Therefore, the addition of surfactant may not be necessary if the dissociated ligands can act as a capping agent, and the reaction is expected to be more reproducible by the elimination of one reaction variable. On the other hand, a weak point of this synthetic method is that the ratio of metal-to-carboxylate ligand is fixed and cannot be adjusted. In the present work we examine this possibility, and find that the extra surfactant is not necessary in this non-hydrolytic synthesis.

SnO_2 is commonly used in transparent conductive electrodes,[18] gas sensors,[19] electrochromic devices,[20] anode materials for batteries,[21] *etc.* Similarly, CeO_2 has a variety of applications, particularly in catalysts,[22] fuel cells,[23] solid electrolytes,[24] *etc.* So far, various strategies have been applied to tailoring the shape and size of SnO_2[25–30] and CeO_2,[31–34] nanoparticles, and the findings here will provide a meaningful contribution in these fields.

Results and discussion

The XRD patterns of the SnO_2 and CeO_2 nanoparticles synthesized by the two-step solvothermal reaction at 290 °C are shown in Fig. 1. The prepared SnO_2 and CeO_2 nanoparticles were of cassiterite and calcium fluoride (CaF_2) structure, respectively. The crystallite size of the SnO_2 nanoparticle,

Department of Chemistry, Inha University, Incheon, 402-751, Korea. E-mail: wanin@inha.ac.kr; Fax: +82 32-867-5604; Tel: +82 32-863-1026

† The HTML version of this article has been enhanced with colour images.

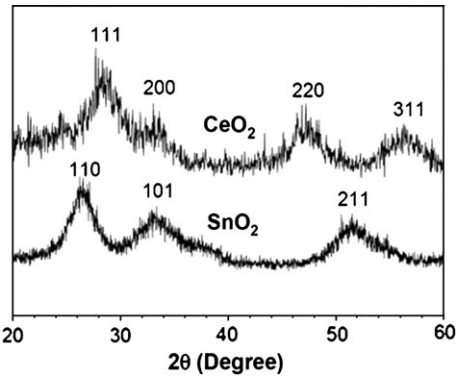

Fig. 1 XRD patterns of the SnO_2 and CeO_2 nanoparticles synthesized by the two-step solvothermal reaction at 290 °C.

calculated from the XRD 110 peak ($2\theta = 26.611°$) by applying the Scherrer equation, was 2.3 nm, while that of the CeO_2 nanoparticle, determined from the 111 peak ($2\theta = 28.549°$), was 2.8 nm.

Fig. 2 shows TEM images of the SnO_2 nanoparticles obtained through the two-step solvothermal reaction at 290 °C. As shown in Fig. 2(a) and 2(b), most of the SnO_2 nanoparticles were spherical in shape, without mutual aggregation. The nanoparticles were monodispersed, and the average particle size was 2.4 nm, which corresponds to the crystallite size calculated from the XRD patterns. The ring patterns of the selective area electron diffraction (SAED) in Fig. 2(c) are assigned to the (110), (101), (211) and (112) planes of the cassiterite phase. Fig. 2(d) shows a high resolution TEM image of a SnO_2 nanoparticle. Uniform fringes, with an interval of 0.34 nm, corresponding to the (110) lattice spacing of the cassiterite phase, were observed over the entire region of the SnO_2 nanoparticle.

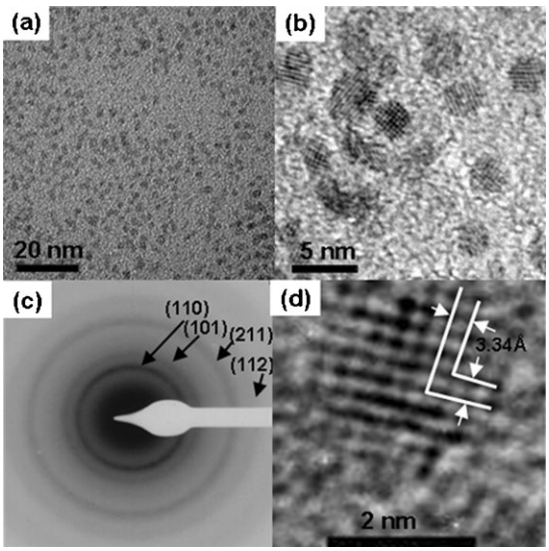

Fig. 2 TEM images of SnO_2 nanoparticles synthesized by the two-step solvothermal reaction at 290 °C. (a/b): Images of SnO_2 nanoparticles spread on a holey carbon grid; (c): SAED patterns; (d): High resolution image.

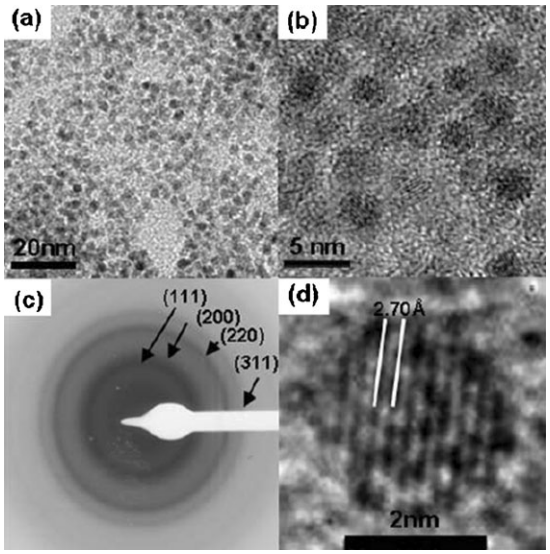

Fig. 3 TEM images of CeO_2 nanoparticles synthesized by the two-step solvothermal reaction at 290 °C. (a/b): Images of CeO_2 nanoparticles spread on a holey carbon grid; (c): SAED patterns; (d): High resolution image.

Fig. 3 shows TEM images of the CeO_2 nanoparticles synthesized at 290 °C. As shown in Fig. 3(a) and 3(b), the CeO_2 nanoparticles are mostly spherical in shape, without any aggregation. The average particle size was 2.6 nm, which is consistent with the crystallite size of 2.8 nm calculated from the XRD patterns. The SAED ring patterns in Fig. 3(c) are identified as (111), (200), (220) and (311) planes of a CeO_2 cubic phase (CaF_2 structure). Fig. 3(d) shows a high resolution TEM image of a CeO_2 nanoparticle. Uniform fringes, with an interval of 2.70 Å, corresponding to the (200) lattice spacing, were observed over the entire region of the SnO_2 nanoparticle.

During the solvothermal reaction, a preliminary reaction at the flash point of the metal carboxylate is crucial for achieving monodispersed nanoparticles. In this preliminary reaction at 113 °C for 3 h, the tin(II) 2-ethylhexanoate or cerium(III) 2-ethylhexanoate complexes thermally decompose, and the 2-ethylhexanoate ligands dissociate into the solution. Then, the released 2-ethylhexanoate ligands in *n*-butylether solution serve as capping agents to the metal oxide nuclei. By a subsequent solvothermal reaction at 290 °C, the nanoparticles are gradually grown from the nuclei initially formed at the flash point. When the precursor solution was directly heated up to 290 °C, without first keeping it at 113 °C, the individual nanoparticles merged to form a rod-like structure, as shown in the TEM image in Fig. 4. Moreover, the obtained SnO_2 nanoparticles were less uniform in size and shape. Under this one-step process at 290 °C, the decomposition reaction of the precursor and grain growth will take place simultaneously. As a result of these competing reactions, the size and shape of the nanoparticles will not be uniform. This observation clearly indicates that precursor decomposition and nanoparticle growth reactions should be separated to obtain monodispersed nanoparticles.[34,35]

We also varied the reaction temperature in the preparation of SnO_2 nanoparticles. After the preliminary reaction at the

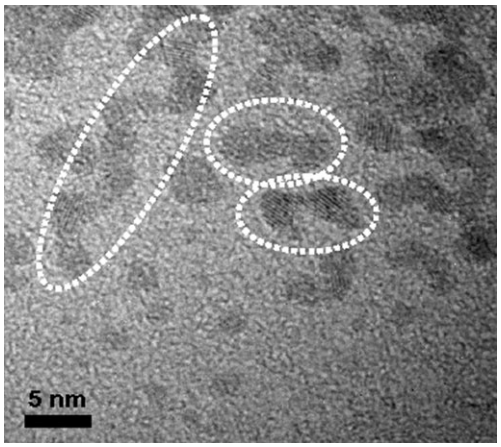

Fig. 4 TEM image of the SnO_2 nanoparticles synthesized by direct heating at 290 °C, without the preliminary reaction at 113 °C.

flash point, the main reaction temperatures were adjusted to 250 and 270 °C, respectively. Compared to the nanoparticles prepared at 290 °C, the SnO_2 nanoparticles obtained at these temperatures were considerably more aggregated, but their size was not appreciably different. Also, the XRD patterns were the same as those obtained at 290 °C. In addition, we changed the reaction time from 1 to 8 h, but no significant difference in particle size was observed.

There is a possibility that the amount of dissociated 2-ethylhexanoate from the decomposition of tin(II) 2-ethylhexanoate may not be optimum for effective capping of the SnO_2 nanoparticles. When two equivalents of 2-ethylhexanoic acid relative to tin(II) 2-ethylhexanoate were added, the shape of the derived SnO_2 nanoparticles was not appreciably changed, as shown in Fig. 5(a). With the addition of four equivalents of 2-ethylhexanoic acid, the obtained SnO_2 end-product (Fig. 5(b)) was relatively less uniform in size and shape. This clearly indicates that the quantity of 2-ethylhexanoate ligands released from the tin(II) 2-ethylhexanoate precursor is already sufficient for the effective capping of the SnO_2 nanoparticles. Thus, extra surfactants are not necessary at all for the derivation of SnO_2 nanoparticles.

XPS measurements were performed to elucidate the oxidation state of Sn and Ce in the SnO_2 and CeO_2 nanoparticles, respectively. The relative peak shifts were corrected by fixing the peak position of contaminant carbon in the XPS instrument at 284.60 eV. Fig. 6(a) shows the high resolution XPS spectrum of Sn 3d in a SnO_2 nanoparticle prepared by the two-step solvothermal reaction at 290 °C. The peak positions of Sn $3d_{5/2}$ and $3d_{3/2}$ were determined as 486.6 and 495.0 eV, respectively. This indicates that the oxidation state of the SnO_2 nanoparticles is close to +4, based on reports that the peak positions of Sn $3d_{5/2}$ and $3d_{3/2}$ are 486.7 and 495.1 eV, respectively, for SnO_2 nanoparticles.[27,36,37] The Ce 3d XPS spectrum for a CeO_2 nanoparticle is shown in Fig. 6(b). The main peak positions of Ce $3d_{5/2}$ and $3d_{3/2}$ are 883.0 and 899.7 eV, respectively. These were assigned to Ce(IV) peaks.[38,39] The oxygen 1s spectrum of CeO_2 nanoparticles is also illustrated in Fig. 6(c). The peak centered at 529.6 eV corresponds to the 1s of O^{2-}. Thus, the binding energies of Ce 3d and O 1s are in agreement with those typical of CeO_2. Overall, the XPS measurement indicates that oxygen is not appreciably deficient in the SnO_2 and CeO_2 nanoparticles, even though they were synthesized under non-hydrolytic conditions.

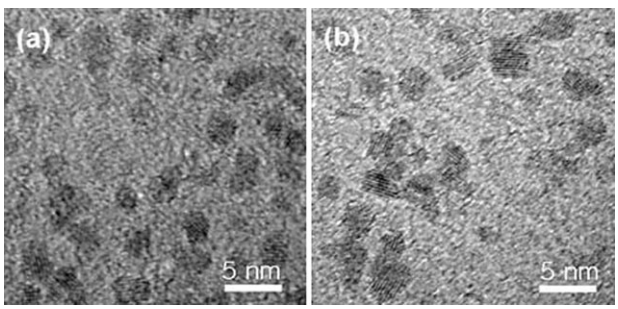

Fig. 5 TEM images of SnO_2 nanoparticles synthesized by the addition of extra 2-ethylhexanoic acid. (a): 2 equivalents of 2-ethylhexanoic acid relative to tin(II) 2-ehtylhexanoate; (b): 4 equivalents of 2-ethylhexanoic acid.

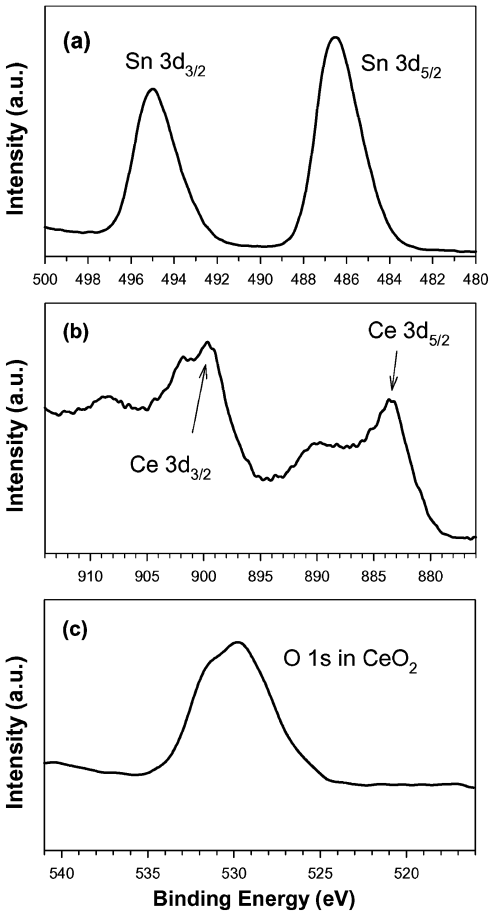

Fig. 6 High resolution XPS spectra of (a) Sn 3d for the SnO_2 nanoparticles, and (b) Ce 3d and (c) O 1s for the CeO_2 nanoparticles synthesized by the two-step solvothermal reaction at 290 °C.

In Fig. 7, the $(\alpha h\nu)^2$ *vs.* photon energy curve, where α is the colloid absorption, h is Planck's constant and ν is the frequency of the light, is plotted for the 2.4 nm-sized SnO_2 and 2.6 nm-sized CeO_2 nanoparticles. The band gap energies for SnO_2 and CeO_2 were determined by extrapolating the tangent of each curve to the x-axis.[40] The band gaps of the SnO_2 and CeO_2 nanoparticles were determined to be 4.14 and 3.68 eV,

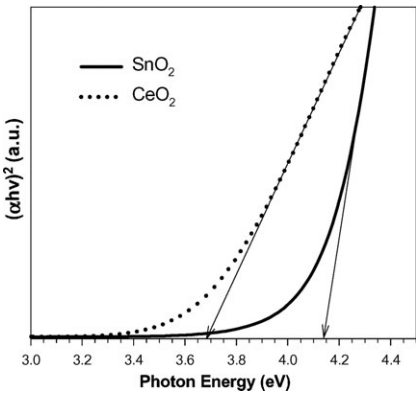

Fig. 7 Absorption onset energy curves for the 2.4 nm-sized SnO_2 and 2.6 nm-sized CeO_2 nanoparticles synthesized by the two-step solvothermal reaction at 290 °C. 5 mg of each nanoparticle was suspended in 5 ml of hexane.

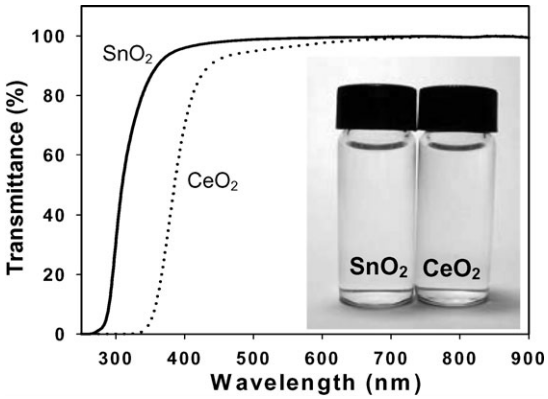

Fig. 8 Transmittance spectra for the citrate-capped SnO_2 and CeO_2 nanoparticles suspended in aqueous solution at pH 12. The concentration of each aqueous suspension was 2 mg ml^{-1} and the optical path length of the suspension in the silica cuvette was 1 cm. The inset shows photographs of the suspensions.

respectively, which are considerably larger than those of bulk SnO_2 (3.62 eV) and CeO_2 (3.19 eV). Also, the obtained values for these nanoparticles are comparatively large among those already reported,[32,41,42] and this is ascribed to the quantum size effect caused by electron-hole confinement.

The synthesized SnO_2 and CeO_2 nanoparticles capped with 2-ethylhexanoate fragments were stably-suspended in a non-polar solvent. That is, suspensions containing 45 mg SnO_2 or 10 mg CeO_2 per 1 ml of *n*-butylether were optically transparent. However, they were instantly precipitated in a polar solvent such as water or ethanol. To convert them to water soluble nanoparticles, 80 ml of ethanol and 4.0 mmol of citric acid were added to 1.0 mmol of dried SnO_2 or CeO_2 nanoparticles, and were then stirred at 80 °C for 3 h. The capped 2-ethylhexanoate groups on the surface of the nanoparticle were gradually exchanged for citrate groups, and citrate-capped nanoparticles were slowly precipitated. The precipitated SnO_2 or CeO_2 nanoparticles were collected by centrifugation, and were washed several times with hexane and then ethanol/water (50/50 volume ratio). The collected precipitate was suspended in water and the pH of the solution adjusted to 11–13 by adding trimethylammonium hydroxide (TMAH). Then, the SnO_2 or CeO_2 nanoparticles were stably-suspended in an aqueous solution. Fig. 8 shows the transmittance spectra of the SnO_2 and CeO_2 nanoparticles suspended in the aqueous solution (2.0 mg ml^{-1}). The transmittance of the SnO_2 aqueous suspension was more than 98% in the visible range, and that of CeO_2 was about 95%. Both are optically transparent, as shown in the inset of Fig. 8. It was also found that the aqueous suspensions kept their optical transparency up to a concentration of $\sim$4 mg ml^{-1}.

As observed, this synthetic method is very simple, provides high reproducibility and enables large scale synthesis at low expense. We expect that this preparation strategy can be extended to the preparation of quantum-sized nanoparticles of various metal oxides.

Conclusions

By means of a two-step solvothermal reaction with 2-ethylhexanoate complexes, highly monodispersed 2.4 nm-sized SnO_2 and 2.6 nm-sized CeO_2 nanoparticles were reproducibly formed. During formation of the nanoparticles, the dissociated 2-ethylhexanoate behaved as a capping agent, and the quantity of 2-ethylhexanoate ligands released from the tin(II) 2-ethylhexanoate precursor was sufficient for effective capping of the SnO_2 nanoparticles. In this solvothermal reaction, a preliminary reaction at the flash point of the metal carboxylate was crucial for achieving monodispersed nanoparticles. This indicated that the reactions of precursor decomposition and nanoparticle growth should be separated to obtain the monodispersed nanoparticles. Even though the nanoparticles were formed under non-hydrolytic conditions, the oxidation state of the Sn and Ce were close to +4, as indicated by XPS analysis. The relatively larger band gaps (SnO_2: 4.14 eV; CeO_2: 3.68 eV) were ascribed to the quantum size effect, which is presumably caused by the smaller particle size and the reduced interparticle aggregation.

Experimental

For the synthesis of SnO_2 nanoparticles, 2.4 mmol of tin(II) 2-ethylhexanoate $[(CH_3(CH_2)_3CH(C_2H_5)CO_2)_2Sn$, 97%, Aldrich Chemical Co.] was dissolved in 10 ml of *n*-butylether (99%, Aldrich Chemical Co.). The clear mixture was stirred for 30 min at 40 °C and then transferred to a glass-lined autoclave. The reaction consisted of the following two-step process. Firstly, the reactor containing the mixture was heated at 113 °C for 3 h to induce decomposition of the 2-ethylhexanoate precursor and nucleation. Secondly, the reaction temperature was raised to 290 °C and held as such for 2 h to allow the growth of nanocrystalline SnO_2. For the preparation of CeO_2 nanoparticles, 0.26 mmol of cerium(III) 2-ethylhexanoate $[(CH_3(CH_2)_3CH(C_2H_5)CO_2)_3Ce$, 97%, Aldrich Chemical Co.] was dissolved in 15 ml of *n*-butylether. Other reaction conditions were the same as those applied to the synthesis of SnO_2 nanoparticles. After the reaction at 290 °C, the SnO_2 or CeO_2 nanoparticles were obtained as transparent colloidal suspensions in *n*-butylether.

To obtain powdered SnO_2 or CeO_2 from the 10 ml *n*-butylether suspensions, 10 ml of ethanol was added. The 2-ethylhexanoate-capped nanoparticles were then slowly precipitated. The precipitated nanoparticles were collected by centrifugation, rinsed with ethanol several times, and then dried in a vacuum oven at room temperature. The dried SnO_2 or CeO_2 nanoparticles capped with 2-ethylhexanoate were readily soluble in non-polar solvents such as toluene or hexane.

To observe the synthesized nanoparticles by TEM (Philips CM30 Transmission Electron Microscope operated at 250 kV), 1 mg of nanoparticles were dispersed in 50 ml of methanol and a drop of the suspension then spread on a holey amorphous carbon film, deposited on a Ni grid (JEOL Ltd.). Optical transmissions of the SnO_2 and CeO_2 suspensions were recorded by a UV-visible spectrophotometer (Perkin-Elmer Lambda 40) in the wavelength range 200–800 nm. X-Ray photoelectron spectroscopy (XPS) analyses of the SnO_2 and CeO_2 nanoparticles were carried out in an ultrahigh vacuum (UHV) chamber with a base pressure below 5×10^{-9} Torr at room temperature. Photoemission spectra were recorded by a Sigma Probe Instrument (Thermo VG, UK) equipped with a standard monochromatic Al-K_α excitation source ($h\nu$ = 1486.6 eV). For the high resolution XPS scan, the pass energy and step size were adjusted to 20 and 0.1 eV, respectively.

Acknowledgements

The authors gratefully acknowledge the financial support provided by Inha University.

References

1 L. O. Brown and J. E. Hutchison, *J. Am. Chem. Soc.*, 1999, **121**, 882.
2 I. Lisiecki, *J. Phys. Chem. B*, 2005, **109**, 12231.
3 C. Sangregorio, M. Galeotti, U. Bardi and P. Baglioni, *Langmuir*, 1996, **12**, 5800.
4 M. P. Pileni, *Langmuir*, 1997, **13**, 3266.
5 (*a*) M. P. Pileni, *Catal. Today*, 2000, **58**, 151; (*b*) B. C. Petit, P. Lixon and M. P. Pileni, *J. Phys. Chem.*, 1990, **94**, 1598.
6 T. Hirai, T. Watanabe and I. Komasawa, *J. Phys. Chem. B*, 2000, **104**, 8962.
7 Y. W. Jun, Y. Y. Jung and J. Cheon, *J. Am. Chem. Soc.*, 2002, **124**, 615.
8 T. Hyeon, S. S. Lee, J. Park, Y. Chung and H. B. Na, *J. Am. Chem. Soc.*, 2001, **123**, 12798.
9 W. S. Seo, H. H. Jo, K. Lee and J. T. Park, *Adv. Mater.*, 2003, **15**, 795.
10 K. Kuppusamy and S. Govindarajan, *Thermochim. Acta*, 1996, **279**, 143.
11 B. N. Sivasankar and S. Govindarajan, *Mater. Res. Bull.*, 1996, **31**, 47.
12 M. Niederberger, M. H. Bartl and G. D. Stucky, *J. Am. Chem. Soc.*, 2002, **124**, 13642.
13 (*a*) G. Garnweitner, M. Antonietti and M. Niederberger, *Chem. Commun.*, 2005, 397; (*b*) G. Garnweitner and M. Niederberger, *J. Am. Ceram. Soc.*, 2006, **89**, 1801; (*c*) M. Niederberger, G. Garnweitner, N. Pinna and G. Neri, *Prog. Solid State Chem.*, 2006, **33**, 59.
14 D. Diaz, M. Rivera, T. Ni, J.-C. Rodriguez, S.-E. Castillo-Blum, D. Nagesha, J. Robles, O.-J. Alvarez-Fregoso and N. A. Kotov, *J. Phys. Chem. B*, 1999, **103**, 9854.
15 K. V. P. M. Shafi, I. Felner, Y. Mastai and A. Gedanken, *J. Phys. Chem. B*, 1999, **103**, 3358.
16 M. Epifani, J. Arbiol, R. Diaz, M. J. Peralvarez, P. Siciliano and J. R. Morante, *Chem. Mater.*, 2005, **17**, 6468.
17 (*a*) A. S. U. Son, Y. K. Jang, Y. Yoon, C. An, Y. Hwang, J. Park, H. Noh, J. Kim, J. Park and T. Hyeon, *Chem. Commun.*, 2005, 86; (*b*) B. E. Kang, J. Park, Y. Hwang, M. Kang, J. Park and T. Hyeon, *J. Phys. Chem. B*, 2004, **108**, 13932.
18 (*a*) A. K. L. Chopra, S. Major and D. K. Pandya, *Thin Solid Films*, 1983, **102**, 1; (*b*) B. C. Goebbert, M. A. Aegerter, D. Burgard, R. Nass and H. Schmidt, *J. Mater. Chem.*, 1999, **9**, 253; (*c*) C. H. Cachet, A. Gamard, G. Campet, B. Jousseaume and T. Toupance, *Thin Solid Films*, 2001, **388**, 41.
19 (*a*) G. Ansari, P. Boroojerdian, S. R. Sainkar, R. N. Karekar, R. C. Aiyer and S. K. Kulkarni, *Thin Solid Films*, 1997, **295**, 271; (*b*) O. K. Varghese and L. K. Malhotra, *Sens. Actuators, B*, 1998, **53**, 19.
20 P. Olivi, E. C. Pereira, E. Longo, J. A. Varella and L. O. Bulhoes, *J. Electrochem. Soc.*, 1993, **140**, L81.
21 J. Zhu, Z. Lu, S. T. Aruna, D. Aurbach and A. Gedanken, *Chem. Mater.*, 2000, **12**, 2557.
22 (*a*) A. G. Jacobs, L. Williams, U. Graham, D. Sparks and B. H. Davis, *J. Phys. Chem. B*, 2003, **107**, 10398; (*b*) M. Asadullah, T. Miyazawa, S. Ito, K. Kunimori and K. Tomishige, *Energy Fuels*, 2003, **17**, 842.
23 Z. C. Kang and Z. L. Wang, *Adv. Mater.*, 2003, **15**, 521.
24 H. Inaba and H. Tagawa, *Solid State Ionics*, 1996, **83**, 1.
25 C. Nayarl, E. Viala, P. Fau, F. Senocq, J. Jumas, A. Maisonnat and B. Chaudret, *Chem.–Eur. J.*, 2000, **6**, 6082.
26 H. Deng, F. J. Lamelas and J. M. Hossenlopp, *Chem. Mater.*, 2003, **15**, 2429.
27 H. J. Ahn, H. C. Choi, K. W. Park, S. B. Kim and Y. E. Sung, *J. Phys. Chem. B*, 2004, **108**, 9815.
28 C. Ribeiro, E. J. H. Lee, T. R. Giraldi, E. Longo, J. A. Varela and E. R. Leite, *J. Phys. Chem. B*, 2004, **108**, 15612.
29 J. Ba, J. Polleux, M. Antonietti and M. Niederberger, *Adv. Mater.*, 2005, **17**, 2509.
30 H. Zhu, D. Yang, G. Yu, H. Zhang and K. Yao, *Nanotechnology*, 2006, **17**, 2386.
31 Y. He, B. Yang and G. Cheng, *Mater. Lett.*, 2003, **57**, 1880.
32 T. Masui, K. Fujiwara, K. Machida and G. Adachi, *Chem. Mater.*, 1997, **9**, 2197.
33 H.-X. Mai, L.-D. Sun, Y.-W. Zhang, R. Si, W. Feng, H.-P. Zhang, H.-C. Liu and C.-H. Yan, *J. Phys. Chem. B*, 2005, **109**, 24380.
34 J. Park, E. Kang, S. U. Son, H. M. Park, M. K. Lee, J. Kim, K. W. Kim, H. Noh, J. Park, C. J. Bae, J. Park and T. Hyeon, *Adv. Mater.*, 2005, **17**, 429.
35 S. Kim, J. Park, Y. Jang, Y. Chung, S. Hwang and T. Hyeon, *Nano Lett.*, 2003, **3**, 1289.
36 J. Hays, A. Punnoose, R. Baldner, M. H. Engelhard, I. Peloquin and K. M. Reddy, *Phys. Rev. B: Condens. Matter Mater. Phys.*, 2005, **72**, 75203.
37 C. Liang, Y. Shimizu, T. Sasaki and N. Koshizaki, *J. Phys. Chem. B*, 2003, **107**, 9220.
38 P. X. Huang, F. Wu, B. L. Zhu, X. P. Gao, H. Y. Zhu, T. Y. Yan, W. P. Huang, S. H. Wu and D. Y. Song, *J. Phys. Chem. B*, 2005, **109**, 19169.
39 A. M. Salvi, F. Decker, F. Varsano and G. Speranza, *Surf. Interface Anal.*, 2001, **31**, 255.
40 F. Gu, S. F. Wang, M. K. Lu, G. J. Zhou, D. Xu and D. R. Yuan, *J. Phys. Chem. B*, 2004, **108**, 8119.
41 (*a*) A. E. De Souza, S. H. Monteiro, C. V. Santilli and S. H. Pulcinelli, *J. Mater. Sci.*, 1997, **8**, 265; (*b*) H. Zhu, D. Yang, G. Yu, H. Zhang and K. Yao, *Nanotechnology*, 2006, **17**, 2386; (*c*) S. Das, S. Kar and S. Chaudhuri, *J. Appl. Phys.*, 2006, **99**, 114303; (*d*) F. Gu, S. F. Wang, M. K. Lu, G. J. Zhou, D. Xu and D. R. Yuan, *J. Phys. Chem. B*, 2004, **108**, 8121; (*e*) G. Pang, S. Chen, Y. Koltypin, A. Zaban, S. Feng and A. Gedanken, *Nano Lett.*, 2001, **1**, 723.
42 (*a*) L. Filotti, A. Bensalem, F. Bozon-Verduraz, G. A. Shafeev and V. V. Voronov, *Appl. Surf. Sci.*, 1997, **109/110**, 249; (*b*) C. Ho, J. C. Yu, T. Kwong, A. C. Mak and S. Lai, *Chem. Mater.*, 2005, **17**, 4514; (*c*) S. Tsunekawa, T. Fukuda and A. Kasuya, *J. Appl. Phys.*, 2000, **87**, 1318.

